EN-SITU EXAFS INVESTIGATION OF ZEOLITE SUPPORTED Pt ELECTROCATALYST STRUCTURE

JUN YAO[1] and YUFENG YAO[2]

Abstract

Experimental investigation was carried out for Pt electrochemical performance and Pt particle size using 1.5 wt% and 5 wt% Pt loading on zeolite electrocatalysts made by $Pt(NH_3)_4(NO_3)_2$ or $Pt(NH_3)_4(NO_3)_2/NH_4NO_3$ salt with ion exchanged method and calcined at 350 ^oC and reduced at 400 ^oC or direct reduced at 400 ^oC, respectively. Cyclic voltammetry measurement indicated that the hydrogen energy binding level on Pt surfaces is higher for electrocatalyst under direct reduction process than those made by calcination and reduction process. The extended X-ray adsorption fine structure measurement revealed that Pt size for electrocatalyst made by calcination and reduction method is smaller than those made by direct reduced method. Furthermore, Pt size for electrocatalysts with 1.5 wt% Pt loading on zeolite is smaller compared to those with 5 wt% Pt loading electrocatalysts. Aforementioned electrochemical performance of Pt zeolite electrocatalysts has depicted by a hypothesis of hydrogen spillover and surface conductance pathway.

KEY WORDS: Platinum nanoparticle; Calcination and reduction; Direct reduction; CO Cyclic voltammetry; Extended X-ray adsorption fine structure; H_2 spillover and surface conductance.

1. Introduction

Zeolite is increasingly employed for fuel cell application due to its chemical and physical characteristics which can offer a crystallized structure with great capacity for containing water. It also can be completely hydrated and dehydrated without damage to the crystalline lattice [1]. These properties are particularly appealing to proton exchange membrane fuel cell (PEMFC) that relies on liquid water to maintain and facilitate fast electrochemical kinetics [2] during electrochemical reaction through a self-humidification process [3]. Moreover, zeolite comprising of $[SiO_4]$ and $[AlO_4]$ tetrahedral structure can bring extra framework of metal cations with interconnection channels to host unique chemistry features [4].

[1] School of Engineering, University of Lincoln, Brayford Pool, Lincoln LN6 7TS, UK, jyao@lincoln.ac.uk
[2] Department of Engineering Design and Mathematics, University of the West of England, Coldharbour Lane, Bristol BS16 1QY, UK, Yufeng.Yao@uwe.ac.uk

It is known that zeolite catalytic performance can be modified by pre-exchange ions to produce a desired cationic form [4]. The metal microstructure constrained within zeolite supercages varies in size from a single atom scale to nanoparticle scale in an order of 1 - 2 nm [5], forming clusters containing 10 - 25 atoms on average [6]. The metal particles supported on zeolite exteriors that are not constrained by zeolite internal architecture and their sizes can still be smaller than micrometer [5, 7].

Past researches have revealed that Pt is a practically important element as catalyst [8] for a variety of electrochemical reactions in acid solution, in which catalytic activity can be promoted on zeolite. A high dispersion of Pt on zeolite was found to be achieved by calcination and reduction steps with oxygen and hydrogen purging in the gas phase under careful temperature control. Pt was mostly located in zeolite supercages under calcination at 350 ^{o}C and reduction at 400 ^{o}C [9]. Zeolite as ionic conductor can act as an electron bank to release electrons to or absorb electrons from a reactant during an electrochemical reaction to provide an ionic conduction [10]. This will lead to an electrochemical reaction occurring in a charger balanced ionic environment like in an electrochemical system [1].

Previously, Rolison *et al.* [5] and Carter et al. [11] have applied an approach using microelectrode by dispersing the modified zeolite powder in an electrolyte solution of high ionic strength placed between two large feeder electrodes. The complication of their methods may induce the Pt nanoparticle exchange coming out of the zeolite structure into the electrolyte solution, and thus circumventing the problem of electronic conduction within zeolite [1, 12].

In order to overcome those difficulties aforementioned, we are proposing to use electrode made by Y zeolite supported Pt samples mixed with XC-72R carbon powder and Nafion$^{@}$ as binding agent, similar to those prepared for polymer electrolyte membrane fuel cells application. Therefore, this paper will be devoted to investigate Pt distribution and the influence of Pt particle size on electron transfer process by increasing the Pt loading from 1.5 wt% to 5 wt% on zeolite using cyclic voltammetry (CV) measurements of CO and hydrogen adsorption and desorption, and moreover the extended X-ray absorption fine structure (EXAFS) technique.

2. Experimental

2.1. 1.5 wt% and 5 wt% Pt/Y zeolite electrocatalysts ion exchanged using $Pt(NH_3)_4(NO_3)_2$ or $Pt(NH_3)_4(NO_3)_2/NH_4NO_3$ salts

Y zeolite was used as a support for the deposition of 1.5 wt% or 5 wt% Pt loadings (as target value), followed by a procedure reported previously in [13, 14]. The 1.5 wt% and 5 wt% Pt loading on Y zeolite electrocatalysts was made by ion exchange method using $Pt(NH_3)_4(NO_3)_2$ salt (denoted as 15Ptancr4 for 1.5 wt% Pt loading and 5Ptancr4 for 5 wt% Pt loading on Y zeolite thereafter) or $Pt(NH_3)_4(NO_3)_2/NH_4NO_3$ salt (denoted as 15Ptanxcr4 for 1.5 wt% Pt loading and 5Ptanxcr4 for 5 wt% Pt loading on Y zeolite thereafter) and calcination and reduction procedure, respectively.

The mechanism of ion replacement on zeolite is to exchange $[Pt(NH_3)_4]^{2+}$ ligand with sodium ion (Na^+) that has an affinity with a negative charge situated on the alumina tetrahedral arrangement $[AlO_4]^-$. One $[Pt(NH_3)_4]^{2+}$ ligand replaces two Na^+ ions to interact with two negative charges situated on two $[AlO_4]^-$ ions resulted in a charge balance. Then, one Pt^{2+} ion bridges with two $[AlO_4]^-$ ions after calcination process to decompose ammonia ligand.

The ion exchange was carried out in a neutral solution at pH 7. An appropriate quantity of $Pt(NH_3)_4(NO_3)_2$ was thoroughly dissolved in 200 *ml* of triply distilled water using an ultrasonic bath at room temperature. The sodium Y zeolite powder was dispersed at a concentration of 1 *g* per 100 *ml* in a water-jacketed reactor, where the Pt ion was slowly added by pumping $Pt(NH_3)_4(NO_3)_2$ salt solution. The sample was then washed with triply distilled water until no $[Pt(NH_3)_4]^{2+}$ complex detected by Ultraviolet (UV) [13]. Sample was later dried overnight in an oven.

In the excess of nitrate ion exchange method using $Pt(NH_3)_4(NO_3)_2/NH_4NO_3$, the NH_4NO_3 was added firstly into the suspended zeolite using stoichiometric titration method to provide a NH_4NO_3 concentration of 0.063 $mol\ dm^{-3}$ prior to the adding of the $Pt(NH_3)_4(NO_3)_2$ salt.

2.2. Calcination and Reduction Reaction or Direct Reduction

The Pt nanostructure on Y zeolite was synthesized by carrying out the calcination and reduction or direct reduction procedure to remove the Pt coordinate ligand. The water moisture in $Pt(NH_3)_4(NO_3)_2$ salt Y zeolite samples were purged by argon at a moderate temperature in a fluidized bed reactor. O_2 gas was then introduced into the reactor to re-heat samples up to 350 ^oC after cooling. The Pt zeolite samples were chemically reduced at a temperature of 400 ^oC by purging with 5% H_2 and 95% N_2 gas mixture to produce a fine Pt distribution on zeolite. An overall oxidation and reduction of Pt on zeolite is illustrated below.

$$[Pt(NH_3)_4]^{2+} + O_2\ (gas) + 2H_2\ (gas) = Pt + 4NH_3\ (gas) + 2H_2O \qquad (1)$$

For sample ion exchanged with NH_4NO_3 salt (prior to the adding of the $Pt(NH_3)_4(NO_3)_2$ salt), the sample was heated at 300 ^oC in argon to produce a fine distribution of the excess H^+ ions on zeolite framework by removal of NH_3 (as displayed by equation 2). The Pt oxidation and reduction reactions after the introducing of $[Pt(NH_3)_4]^{2+}$ ions were followed by the same procedure described above.

$$NH_4^+ = H^+ + NH_3 \qquad (2)$$

For direct reaction, the 5% H_2/95% N_2 gas mixture was direct introduced into a fluidized reactor at 400 ^oC to decompose $[Pt(NH_3)_4]^{2+}$ complex that was ion exchanged into zeolite channel using $Pt(NH_3)_4(NO_3)_2$ salt (denoted as 5Ptandr4 thereafter).

2.3. Electrochemical Cell and Cyclic Voltammetry

The electrodes were prepared by dispersing a known amount of 1.5 wt% or 5 wt% Pt/Y zeolite samples and untreated XC-72R plain carbon powder mixed with 15 wt% Nafion$^@$ on a carbon black (Vulcan XC-72R) paper hot pressed to dry out water moisture. The resultant electrode was later tested to determine Pt electrocatalytical activity by potential cycling method using potentiostat in a saturated 2.5 mol dm^{-3} H_2SO_4 solution at a scan rate of 1 mV s^{-1} until a stable state of cyclic voltammetry

(CV) obtained. An electrochemical cell employed for CV measurement consists of a Pt/Y zeolite working electrode, an Hg/Hg_2SO_4 Mercury/Mercuries Sulphate (MMS) reference electrode and a Pt gauze counter electrode. The electric current density was measured correspondent to an electrode disc of 2.5 cm^2.

The electrochemically assessable Pt surface areas were measured using carbon oxide (CO) adsorption and electrooxidation process, as the ratio of absorbed CO to Pt active sites was found to be unity at a full CO coverage [15]. CO absorption and stripping voltammogram was conducted in 2.5 mol dm^{-3} H_2SO_4 solutions at ambient room temperature by bubbling CO for 45 minutes at -0.55 V. The dissolved CO was then stripped off on the Pt surface by purging Ar under potential cycling at a scan rate of 1 mV s^{-1}.

2.4. The En-situ Extended X-ray Adsorption Fine Structure Measurement

Pt particles were characterized by the en-situ extended X-ray adsorption fine structure (EXAFS) using a Synchrotron Radiation Source (SRS) at STFC Daresbury National Laboratory [13]. The wiggler beam line was operated at conditions of 2 *GeV* and 100 *mA*. High-order harmonics that might affect the amplitude of EXAFS were removed using a double-crystal Si220 monochromator. The 50% detuning of harmonic beam using gas ion chambers filled with Ar, Xe or Kr and He was used to locate the Pt L_{III} absorption edge. A Pt foil was used as a reference sample for EXAFS data collection [13, 14].

EXAFS data was collected using a pellet placed in a gas cell, purged with Argon (Ar). The pellet was made by the catalyst powder mixed with boron nitride to give a Pt loading of 0.73 mg cm^{-2}. The resultant EXAFS data was later analyzed using software EXCURV 98.

3. Results and Discussion

3.1. Pt surface area measurement by CO oxidation and stripping process

The total electrochemically accessible Pt surface area on the electrode was measured by CO adsorption and electrooxidation process. Pt particle number is found dependent on CO stripping peaks [16], as the ratio of adsorbed CO to Pt sites is known to be unity at a full CO coverage [15].

Figure 1 depicts a CV comparison for CO adsorption and stripping peaks on the Pt surface using 1.5 wt% or 5 wt% Pt loading on carbon Nafion$^{@}$ bound electrodes made by 40 wt% Pt on carbon with extra XR-72R carbon powder (thereafter denoted as 15PtXC-72R and 5PtXC-72R, respectively). The solid line represents the cyclic voltammogram of CO stripping off on the Pt surface and dashed line depicts results after CO stripping at a scan rate of 1 mV s^{-1} in a 2.5 mol dm^{-3} H_2SO_4 solution. The current density corresponding to the hydrogen desorption is not found, mainly due to the hydrogen adsorption being suppressed at a full CO coverage on the Pt surface. Two CO stripping peaks were captured in a potential region of 0 V and 0.17 V for electrode 15PtXC-72R, corresponding to a single CV stripping peak measured at 0.045 V for electrode 5PtXC-72R (represented by solid line). The formation of Pt oxide might also be involved in CO stripping reaction, as the oxidation of CO happens at a potential where the formation of Pt oxide occurs [17]. The two electrons are transferred in the electrooxidation of one CO molecule and CO stripping peak. The hydride region was re-emerged after CO stripping off on the Pt surface with a single hydrogen peak measured in hydride regions for electrode 15PtXC-72R (represented by dashed line). The hydrogen energy binding level for re-oxidation and desorption on the Pt active sites was found very similar for electrode 15PtXC-72R. The hydride region corresponding to weakly and/or strongly hydrogen adsorption peaks, and as well as hydrogen re-oxidation and desorption peaks are clearly visible for electrode 5PtXC-72R.

The CV measurements for 5 wt% Pt loading on Y zeolite electrodes has shown a similar tendency as to that of carbon electrodes, as depicted in Figure 2. CO stripping peaks were detected at 0.21 V and 0.24 V for electrodes 5Ptancr4 and 5Ptandr4,

respectively. Multiple CO stripping peaks were also captured at -0.24 V and 0.25 V for electrode 5Ptanxcr4. This indicated that the Pt cluster consists of multiple Pt active sites owing to different energy binding levels at which Pt active sites for catalyst with excess H^+ ion was found low, compared to those of catalysts made without excess H^+ ions. The hydrogen adsorption, evaluation and hydrogen desorption peaks were observed in a potential region of -0.5 V and -0.65 V for an electrode 5Ptanxcr4. There were no visible hydrogen adsorption and desorption peaks captured for electrodes 5Ptancr4 and 5Ptandr4 after CO stripping process.

The issue raised for CO measurement of Pt surface area is concerned by CO diffusion process to hardly access those Pt sites encapsulated in zeolite small cages, i.e. sodalite or hexagonal cages, whilst compared to the mobility of hydrogen ion in zeolite channel. Therefore, Pt active surface areas were also determined via hydrogen adsorption peaks.

Table 1 shows a comparison of Pt active surface area determined by following measurements: (1) CO diffusion and (2) hydrogen adsorption and re-oxidation processes. For 5 wt% Pt loading on zeolite electrocatalysts, the CO measurement has shown that Pt active surface area of catalyst 5PtXC-72R is the largest at 28.24 m^2g^{-1}, followed by catalyst 5Ptanxcr4 at 24.29 m^2g^{-1} and catalyst 5Ptancr4 at 20.20 m^2g^{-1}, respectively. Nevertheless, the catalyst 5Ptandr4 made by direct reduction has shown a minimum surface area of 2.89 m^2g^{-1}. Pt active surface area measured by hydrogen adsorption peaks was found higher than those predicted via CO adsorption peaks. The detection of increasing the Pt active surface area by hydrogen adsorption peaks indicated that some of Pt might be encapsulated in zeolite small cages, i.e. sodalite cage, via Pt migration through zeolite channels. In general, Pt particles in those locations are hardly accessed by CO diffusion for electrochemical active surface area (EASA) measurement using CO adsorption method, whereas H^+ ions enable to migrate more easily through zeolite channels. Pt active surface area of catalyst 5Ptanxcr4 determined by hydrogen adsorption and re-oxidation process was found the highest, followed by catalyst 5Ptancr4 and 5Ptandr4, respectively. This observation indicated that Pt particle size made by hydrogen direct reduced method was larger, compared to catalysts 5Ptanxcr4 or 5Ptancr4 under calcination and reduction method.

Figure 3 depicts CV measurements to determine the Pt active surface area for 1.5 wt% loading on zeolite via CO adsorption and stripping process. CO stripping peaks were captured at 0.18 V and 0.28 V for catalysts 15Ptancr4 and 15Ptanxcr4, respectively. Pt active surface area for catalyst 15Ptanxcr4 (see Table 1) was measured the greatest at 96.80 m^2g^{-1}, followed by 40.02 m^2g^{-1} for 15Ptancr4 and 35.47 m^2g^{1} for 15PtXC-72R. The accessible Pt active sites determined by hydrogen adsorption peak area was found having slightly increase in surface area measured at 103.57 m^2g^{-1} for catalysts 15Ptanxcr4 and 51.29 m^2g^{-1} for 15Ptancr4, respectively. The tendency of surface area increase was found similar to those determined for zeolite catalysts with 5 wt% Pt loading on zeolite. Pt active surface areas entrapped in small cages enable to be detected by hydrogen adsorption peaks, whereas it is difficult accessible via CO diffusion process.

It is clearly that the Pt deposition method has a significant effect on the performance of catalyst. Either 1.5 wt% or 5 wt% catalyst made with the excess of H^+ ions presence displays a high Pt active surface area than those made by without excess H^+ ions participating. Pt active surface area given by direct reduction method is the lowest, compared to those made by calcination and reduction method. CO adsorption and stripping process is primarily a surface phenomenon for detection of Pt active sites on the exterior of zeolite. This may be contributed by CO molecule that is too large to diffuse through zeolite interconnection channels to access the Pt active sites encaged within zeolite structure. Therefore, it might be more accurate to measure the electrochemically active surface areas (EASAs) of Pt using hydrogen adsorption on Pt surface. It was found that the H^+ ions could spillover through zeolite active sites by the formation of H_{ads} atom at first and then transmitting H species along zeolite channel to increase the surface conductance of zeolite substrate [18, 19]. H^+ ions have been regarded as one of the most important species in this process [18]. This will result in a flow of protons along the zeolite acidic sites and transports the hydrogen species to the neighbouring Pt particles on zeolite. Therefore, Pt can be electrochemically accessible. Pt particle encapsulated within zeolite structure can be electrochemically reduced via hydrogen spillover process.

The hydrogen measurement of Pt surface area for samples 15XC-72R (i.e. 48.25 m^2g^{-1}) and 5XC-72R (i.e. 30.5 m^2g^{-1}) made by 40 wt% Pt on XC-72R carbon with extra

carbon powder has not shown a great increase, compared to Pt zeolite samples. This implies Pt particle size might not be smaller than Pt zeolite samples due to the difference of carbon powder and zeolite martial properties.

1.5 wt% Pt loading on zeolite catalysts has presented generally high Pt surface area distributions on zeolite in comparison to that of 5 wt% Pt loading on zeolite. Pt particle size might be small at low Pt loading. The increase of Pt loading can cause the sintering of Pt to produce large Pt particle size. Both the Pt particle size and structure were further investigated using the extended X-ray adsorption fine structure described below.

3.2. The en-situ EXAFS measurement for 5 wt% Pt loading on zeolite catalyst by hydrogen chemical reduction

Pt particle size and its structure of 5 wt% Pt loading on zeolite were further investigated by the en-situ EXAFS measurement.

Figure 4 illustrates the EXAFS Chi data and their Fourier transform fitting results. The data were collected at Pt L_{III} edge following hydrogen chemical reduction at ambient room temperature. The fitting results are presented in Table 2. For catalysts 5Ptanxcr4 and 5Ptandr4, Chi data were valid over the range of wave vectors from 2 $Å^1$ to 16.5 $Å^{-1}$, respectively and for 5Ptancr4 it was only valid up to 14.5 $Å^{-1}$. The curve fitting matched raw measurement data very well. Pt coordination number in the Pt-Pt first shell for catalyst 5Ptandr4 predicated at 8.31 was found greater than those of catalysts 5Ptancr4 predicted at 7.47 and 5Ptanxcr4 at 6.02, respectively. The fitting of Pt shells was extended up to the Pt-Pt fourth shell for all catalysts with an averaged total of Pt atoms predicted at 19, 18 and 25 for catalysts 5Ptancr4, 5Ptanxcr4 and 5Ptandr4, respectively. A Pt-O first shell was also fitted for catalyst 5Ptanxcr4 with coordination number predicted at 0.55 and the Pt-O was fitted at 1.93 Å. The Pt-Pt distances were predicted at 2.76 *Å* for catalysts 5Ptanxcr4 and 5Ptancr4 and 2.75 Å for 5Ptandr4, which were consistent to fitting results for catalysts made by 1.5 wt% Pt loading on zeolite catalyst [13]. The present measurement data supports that Pt has metallic characteristics, which is agreed well with published results by Koningsberger *et al.* [20, 21].

The evaluated particle size can be determined by Benfield theory [22] using equations 3 and 4 to calculate the total Pt atoms in a cluster:

$$\overline{N}_{T(total)} = (1/3)(2m-1)(5m^2-5m+3) \qquad (3)$$

The total surface atoms in a Pt cluster are estimated by the calculation of Pt first shell coordination numbers using the following formulae:

$$\overline{N}_1 = 6[(20m^2-25m+12)]/[(2m-1)(5m^2-5m+3)] \qquad (4)$$

where m = 3 for samples 5Ptancr4 and 5Ptandr4; m = 2 for 15Ptancr4, 15Ptanxcr4 and 5Ptanxcr4. The m value and both of total Pt atoms and surface atoms in a Pt cluster are estimated, based on the Pt first shell refinement value given by the en-situ EXAFS data analysis and the Pt first shell mean value of $\overline{N}_1$ (see Table 3).

It is found proportional to the number of atoms in a cluster, as shown in Table 3. Pt particle for catalysts 5Ptancr4 and 5Ptandr4 consists of a total of 55 atoms in a cluster that is larger than catalysts 5Ptanxcr4 and 15Ptancr4 containing 13 atoms. The catalyst 15Ptanxcr4 has 12 atoms in a Pt cluster. The total surface atoms determined by Benfield method [22] are 42 for catalysts 5Ptancr4 and 5Ptandr4 and 12 for catalysts 15Ptancr4 and 15Ptanxcr4 or 5Ptanxcr4, respectively. The average Pt particle size for 5 wt% Pt zeolite catalysts, i.e. 5Ptancr4 and 5Ptandr4, was estimated at 1.0 – 2.0 nm. Pt particle sizes for catalysts made by excess H^+ ions, i.e. 15Ptanxcr4 and 5Ptanxcr4, are generally smaller than those made without excess H^+ ions presence, i.e. 15Ptancr4, 5Ptancr4 and 5Ptandr4. Pt particle size of catalyst 15Ptanxcr4 estimated at 0.5 – 0.65 nm [13, 14] is the smallest, compared to catalysts 15Ptancr4 and 5Ptanxcr4 for which particle sizes were predicted at 0.8 – 1.0 nm [13, 14]. This finding demonstrates that the presence of H^+ ions can facilitate to achieve a high Pt distribution by anchoring Pt on zeolite specific active sites.

3.3. Comparison

Figure 5 depicts Pt particle distribution (N_S/N_T) determined by total surface atoms of Pt (N_S) over total Pt atoms (N_T) on the per cm^2 of electrode against percentage of actual Pt loading (wt%) on zeolite, calculated by the use of the edge jump from the EXAFS data background subtraction. The Pt dispersion for different types of catalysts is also compared in Table 4. The catalyst 15Ptanxcr4 made by 1.5 wt% Pt loading on zeolite with the excess H^+ ion has presented the highest Pt distribution on zeolite with the minimum actual Pt loading. Pt particle distribution on zeolite follows an order of 15Ptanxcr4 > 15Ptancr4 > 5Ptanxcr4 > 5Ptancr4 > 5Ptandr4, corresponding to a tendency of Pt loading as 15Ptanxcr4 < 15Ptancr4 < 5Ptanxcr4 < 5Ptandr4 < 5Ptancr4. In general, the lower Pt quantity is able to provide a relatively higher Pt distribution on zeolite. The excess H^+ ions can facilitate to achieve higher Pt distribution throughout zeolite channels with generally small Pt particle sizes. The catalysts, i.e. 15Ptanxcr4, 15Ptancr4 or 5Ptanxcr4, have shown a high mobility to migrate Pt through zeolite channels, compared to those with relatively large Pt particle size, i.e. catalysts 5Ptancr4 and 5Ptandr4. For catalyst 5Ptandr4, Pt particle is mainly located on the exterior of zeolite surface, resulting in a shell-like Pt distribution on zeolite surface.

The analytical results have demonstrated that both the Pt particle resided inside the zeolite structure as well as those located on the exterior of zeolite surface can be electrochemically accessible regardless of zeolite being an electronic insulator. In this scenario, the zeolite acts as an electron bank to release or absorb electrons during the electrochemical process. The electrocatalysts with higher Pt particle distribution of smaller sizes is shown to have a better electrochemical performance.

4. Conclusion

The study has shown 1.5 wt% and 5 wt% Pt loading on zeolite catalysts, prepared by $[Pt(NH_3)_4]^{2+}/NH_4^+$, are more favorably located on zeolite supercages or sodalite cages by migration through zeolite channels due to the presence of H^+ ions assisting to anchor Pt particle onto the zeolite cage walls, i.e. catalysts 15Ptanxcr4 and 5Ptanxcr4. Pt particle for catalysts made by $[Pt(NH_3)_4]^{2+}$ with no excess NH_4^+ ions, i.e. 5Ptancr4

and 5Ptandr4, are most likely located at zeolite exterior surface to form a shell-like Pt distribution on zeolite surface. Pt particle size of catalysts with excess protons presence is found smaller but with higher distribution on zeolite structure. This observation confirms that the electrochemical performance can be enhanced by improving Pt distribution on catalyst supporting substrate with an appreciate chemical oxidation and reduction process, and the electrochemical reaction can occur via surface conductance and hydrogen spillover through zeolite channels regardless of zeolite being an electronic DC insulator.

5. References

1. D.R. Rolison, Zeolite-modified electrodes and electrode-modified zeolites, Chemical Review, 1990, 90(5): 867-878.

2. K. Schmidt-Rohr, Q. Chen, Parallel cylindrical water nanochannels in Nafion fuel-cell membranes, Nature Material, 2008, 7: 75-83.

3. D.H. Son, R.K. Sharma, Y.G. Shul, H. Kim, Preparation of Pt/zeolite–Nafion composite membranes for self-humidifying polymer electrolyte fuel cells, J. Power Sources, 2007, 165, 733-738.

4. M.Y. Li, Industry Catalysis Principle, 1992, Tianjin University Publication (in Chinese).

5. D.R. Rolison, E.A. Hayes, W.E. Rudzinski, Electrode-modified zeolites: electrode microstructures contained in and on a heterogeneous catalyst, The Journal of Physical Chemistry, 1989, 93(14): 5524-5531.

6. B.I. Boyanov, T.I. Morrison, Support and Temperature Effects in Platinum Clusters. 1. Spatial Structure, J. Phys. Chem. 1996, 100(40):16310-16317.

7. M. Fleischmann, S. Pons, D.R. Rolison, P.P. Schmidt (eds), Ultramicroelectrodes; Datatech Science Inc. Morganton, NC. 1987.

8. N. Watari, S. Ohnishi, Electronic structure of H adsorbed on Pt13 clusters , J. Chemical Physics, 1997, 106(18): 7531-7540.

9. M.S. Tzou, B.K. Teo, W.M.H. Sachtler, Formation of Pt particles in Y-type zeolites: The influence of coexchanged metal cations, J. Catal., 1988, 113(1): 220-235.

10. D.W. Breck, Zeolite Molecular Sieves: Structure, Chemistry and Use, 1974, John Wiley & Sons Inc: New York.

11. F.L. Carter, R.E. Siatkowski, H. Wohltjen, Molecular Electronic Devices III, 1988, Elsevier: Amsterdam.

12. J.P. Pereira-Ramos. R. Messina, J. Perichon, Electrochemical behaviour of a silver-exchanged “mordenite”-type zeolite, J. Electroanal. Chem. and Interfacial Electrochem., 1983, 146(1): 157-169.

13. J. Yao, Y.F. Yao, Experimental study of characteristics of bimetallic Pt-Fe nano particle fuel cell electrocatalyst, Renewable Energy, 2015, 81: 182-196.

14. J. Yao, Y.F. Yao, Investigation of zeolite supported platinum electrocatalyst for electrochemical oxidation of small organic species, International Journal of Hydrogen Energy, 2016, 41(33):14747-14767.

15. H. Igarashi, T. Fujino, M. Watanabe, Hydrogen electro-oxidation on platinum catalysts in the presence of trace carbon monoxide, J. of Electroanalytical Chemistry and Interfacial Electrochemistry, 1995, 391(1-2): 119-123.

16. B. Beden, S. Bilmes, C. Lamy, J.M. Leger, Electrosorption of carbon monoxide on platinum single crystals in perchloric acid medium, J. Electroanal. Chem. and Interfacial Electrochemistry, 1983, 149(1-2): 295-302.

17. K. Kunimatsu, The infrared spectrum of linearly adsorbed co species produced by chemisorption of methanol on a smooth platinum electrode at high anodic potentials, J. Electroanal. Chem. and interfacial electrochemistry, 1983, 145(1): 219-224.

18. J.M. Herrmann, P. Pichat, Evidence by Electrical Conductivity Measurements for Hydrogen Spill Over on Pt, Rh and Ni/TiO2 Catalysts. Consequences for Bifunctional Photocatalysis, Studies in Surface Science and Catalysis, 1983, 17: 77-87.

19. A. Zhang, I. Nakamura, K. Fujimoto, A New Probe Reaction for Studying the Hydrogen Spillover Phenomenon, J. Catalysis, 1997, 168(2):328-333.

20. D.C. Koningsberger, J.de Graaf, B.L. Mojet, D.E. Ramaker, J.T. Miller, The metal–support interaction in Pt/Y zeolite: evidence for a shift in energy of metal d-valence orbitals by Pt–H shape resonance and atomic XAFS spectroscopy, Applied Catalysis A: General, 2000, 191(1-2): 205-220.

21. M. Vaarkamp, F.S. Modica, J.T. Miller, D.C. Koningsberger, Influence of Hydrogen Pretreatment on the Structure of the Metal-Support Interface in Pt/Zeolite Catalysts, J. of Catalysis, 1993, 144(2): 611-626.

22. R.E. Benfield, Mean coordination numbers and the non-metal–metal transition in clusters, J. of the Chemical Society, Faraday Transactions, 1992, 88(8):1107-1110.

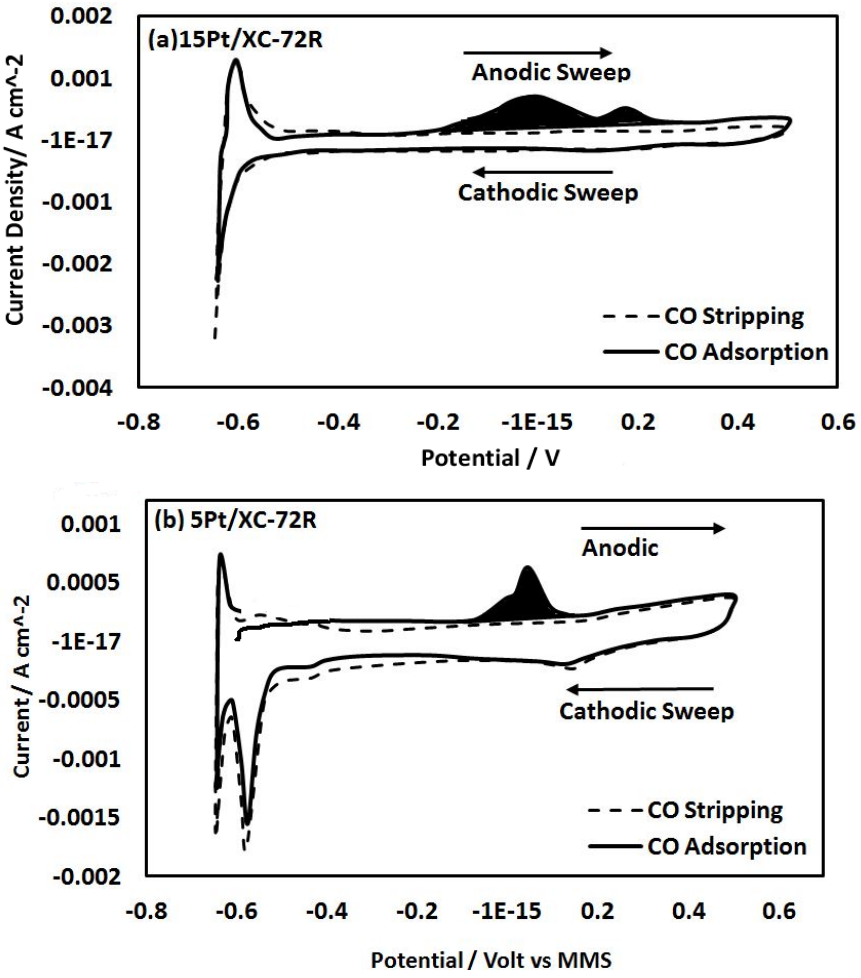

Figure 1. Steady state CV curves of CO oxidation and stripping off on the Pt surface for 1.5 wt% and 5 wt% Pt/XC-72R electrodes at a scan rate of 1 mV s^{-1} in 2.5 mol dm^{-3} H_2SO_4 vs MMS reference electrode. The solid line represents CV measurement of CO oxidation and stripping on the Pt surface, and the dashed line represents CV measurement after CO stripping: (a) 15Pt/XC-72R; (b) 5PtXC-72R.

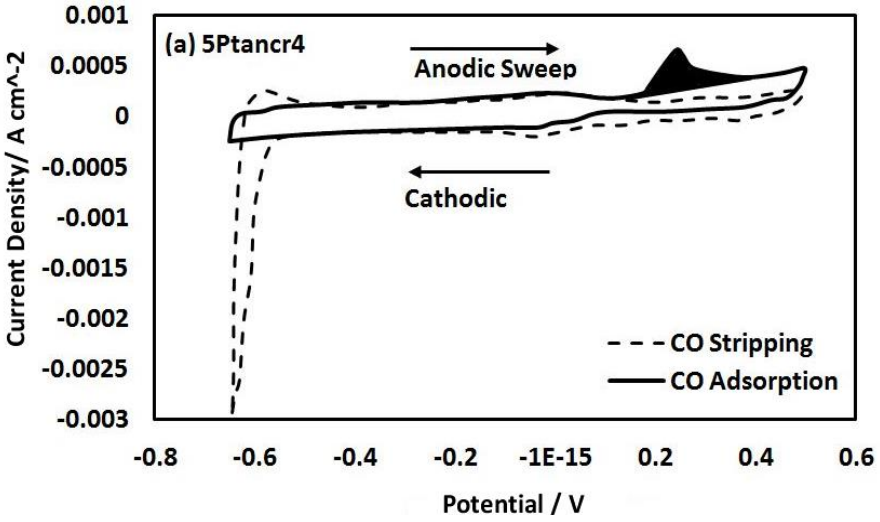

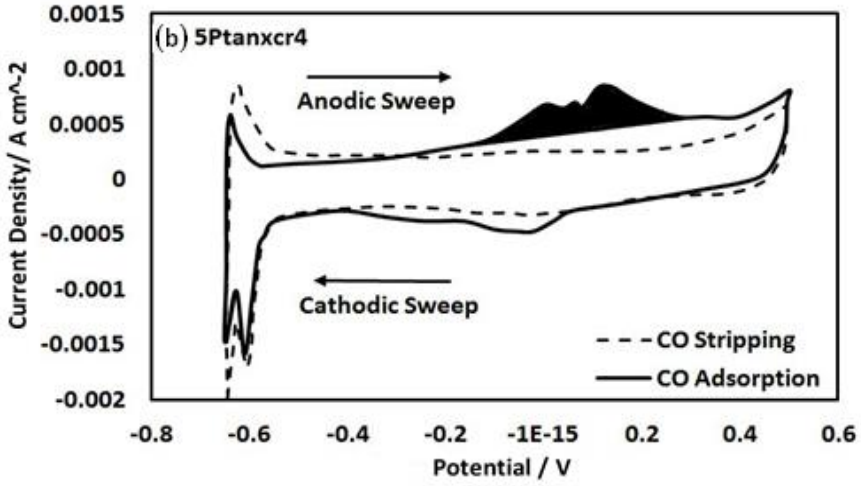

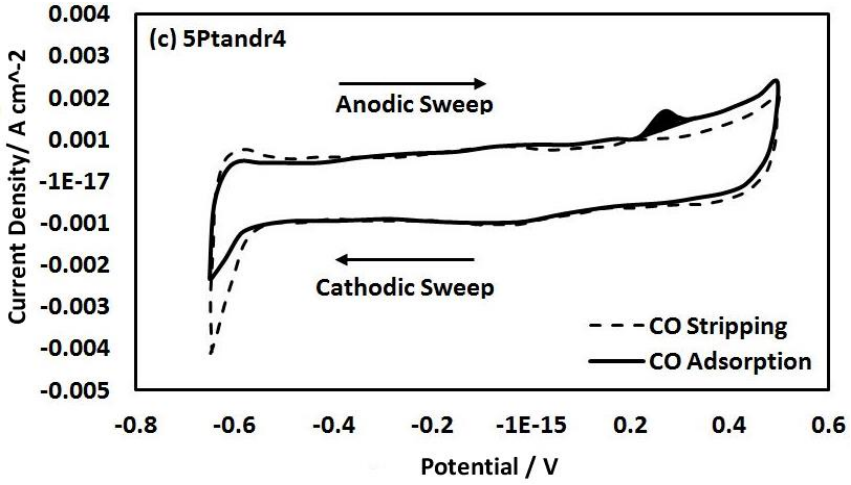

Figure 2. Steady state CV curves of CO oxidation and stripping off on the Pt surface for 5 wt% Pt zeolite electrodes at a scan rate of 1 mV s^{-1} in 2.5 mol dm^{-3} H_2SO_4 vs

MMS reference electrode. The solid line represents CV measurement of CO oxidation and stripping on the Pt surface, and the dashed line represents CV measurement after CO stripping: (a) 5Ptancr4; (b) 5Ptanxcr4; (c) 5Ptandr4.

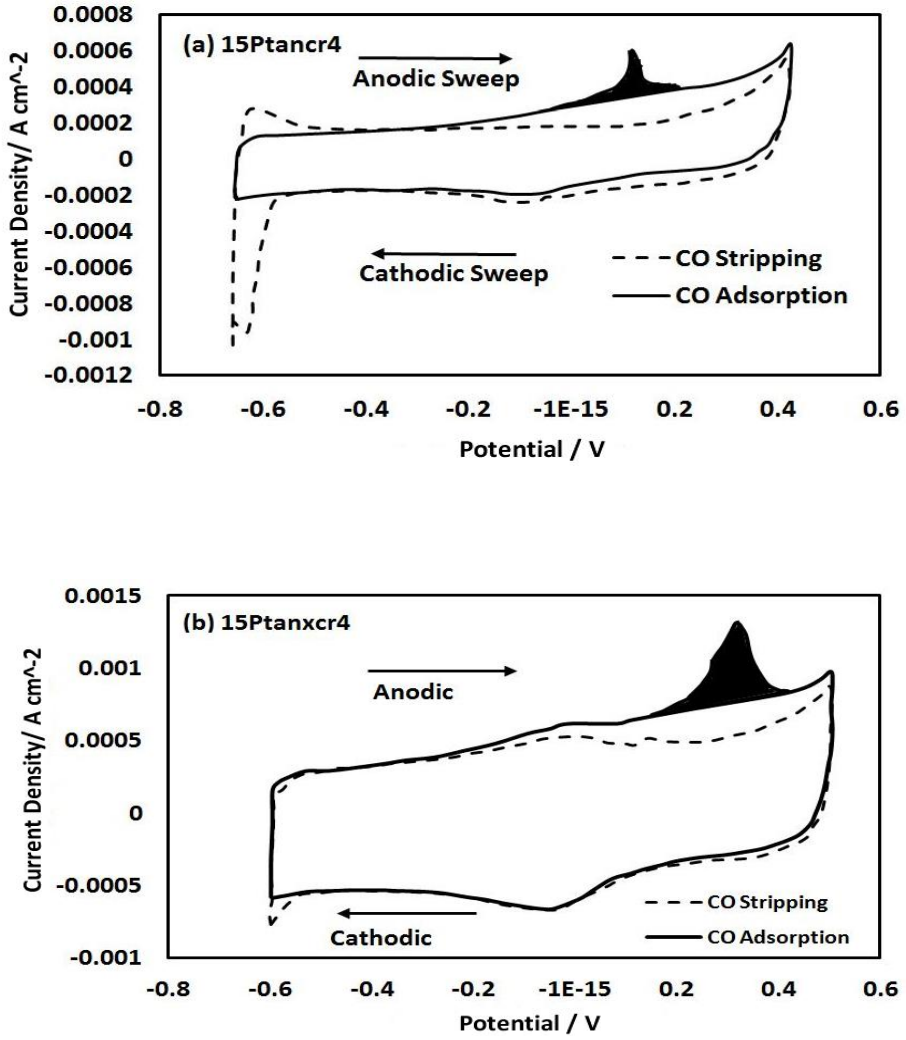

Figure 3. Steady state CV curves of CO oxidation and stripping off on the Pt surface for 1.5 wt% Pt zeolite electrodes at a scan rate of 1 mV s^{-1} in 2.5 mol dm^{-3} H_2SO_4 solution vs MMS reference electrode. The solid line represents CV measurement of CO oxidation and stripping on the Pt surface, and the dashed line represents CV measurement after CO stripping: (a) 15Ptancr4; (b) 15Ptanxcr4.

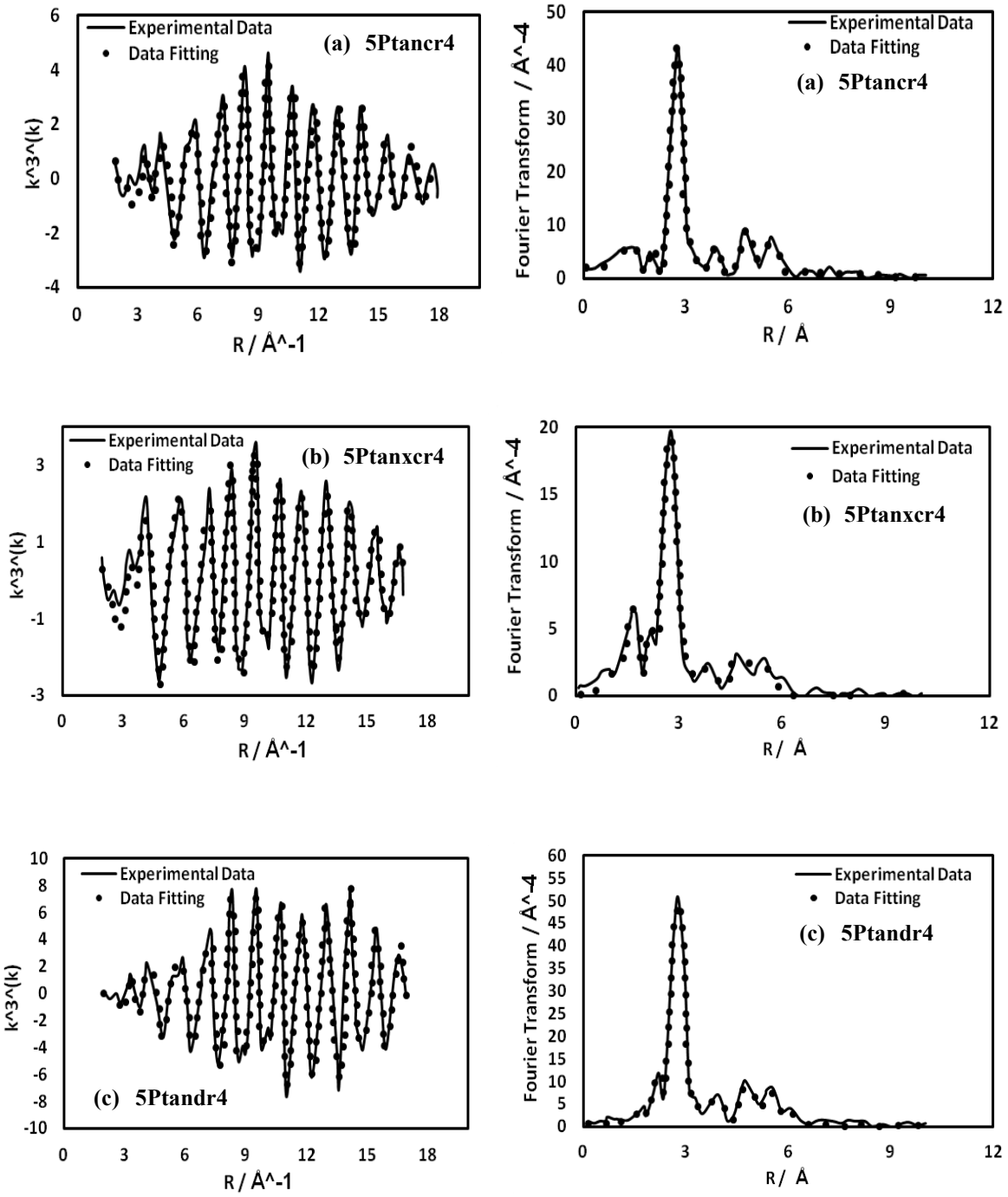

Figure 4. Chi data and Fourier transform for 5 wt% Pt/Y zeolite catalysts, phase corrected. The data were collected at Pt L_{III} edge at ambient room temperature with hydrogen chemical reduction. The solid lines are experimental data, and the dashed lines are the fitted data: (a) 5Ptancr4; (b) 5Ptanxcr4; (c) 5Ptandr4.

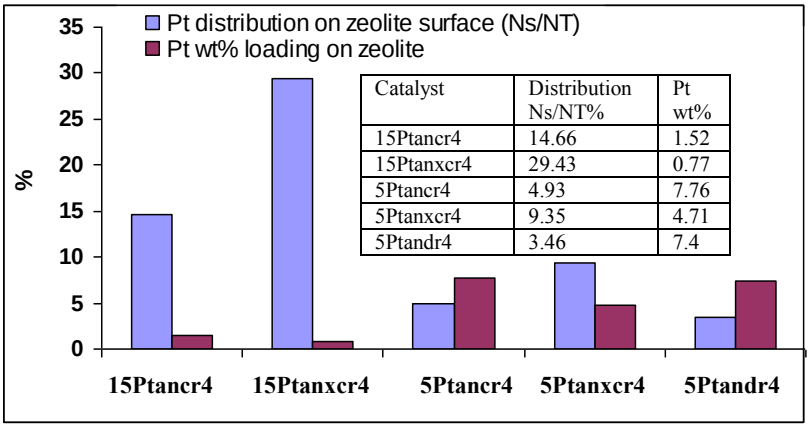

Catalyst	Distribution Ns/NT%	Pt wt%
15Ptancr4	14.66	1.52
15Ptanxcr4	29.43	0.77
5Ptancr4	4.93	7.76
5Ptanxcr4	9.35	4.71
5Ptandr4	3.46	7.4

Figure 5. Comparison of Pt distribution and actual Pt loading on zeolite with catalysts made with or without excess H^+ ions presence under calcination and reduction or direct reduction methods, respectively.

Table 1. Pt active surface area measurement in a potential region of -0.65 V to 0.5 V vs MMS reference electrode.

(a) 5 wt% Pt loading on zeolite electrocatalyst

Catalyst	Pt active surface area (m^2g^{-1}) measured by CO	Pt active surface area (m^2g^{-1}) measured by hydrogen adsorption [14]
5Ptancr4	20.20	21.47
5Ptanxcr4	24.29	32.61
5Ptandr4	2.89	12.05
5PtXC-72R	28.24	30.5

(b) 1.5 wt% Pt loading on zeolite electrocatalyst

Catalyst	Pt active surface area (m^2g^{-1}) measured by CO	Pt active surface area (m^2g^{-1}) measured by hydrogen adsorption [13]
15Ptancr4	40.02	51.29
15Ptanxcr4	96.80	103.57
15PtXC-72R	35.47	48.25

Table 2. EXAFS data fitting results at Pt L_{III} edge for catalysts chemically reduced by gas phase hydrogen at room temperature

(a) catalyst 5Ptancr4

5Ptancr4	N	R/ Å
Shell 1 Pt	7.47±0.12	2.75±0.003
Shell 2 Pt	0.47±0.16	3.88±0.013
Shell 3 Pt	4.53±0.95	4.79±0.015
Shell 4 Pt	6.57±1.50	5.45±0.014

(b) catalyst 5Ptanxcr4

5Ptanxcr4	N	R/ Å
Shell 1 O	0.56±0.12	1.93±0.020
Shell 1 Pt	6.02±0.14	2.75±0.002
Shell 2 Pt	1.81±0.50	3.89±0.015
Shell 3 Pt	4.33±0.70	4.78±0.010
Shell 4 Pt	5.93±1.18	5.42±0.025

(c) catalyst 5Ptandr4

5Ptandr4	N	R/ Å
Shell 1 Pt	8.31±0.15	2.76±0.001
Shell 2 Pt	3.03±0.43	3.91±0.007
Shell 3 Pt	6.28±0.57	4.79±0.004
Shell 4 Pt	7.49±0.98	5.45±0.006

Table 3. Total Pt surface atoms and total Pt atoms in a Pt cluster determined by Benfield theory [22]

Acronym Name	$\overline{N_1}$ from refinement by EXAFS analysis (Pt first shell coordination number)	$\overline{N_s}$ from Benfield's formula (Total number of surface atom in a cluster	$\overline{N_T}$ total number of atoms in a cluster
5Ptancr4	7.47	42	55
5Ptanxcr4[b]	6.02	12	13
5Ptandr4	8.31	42	55
15Ptancr4[13,14]	6.33	12	13
15Ptanxcr4[b] [13, 14]	6.00	12	12

[b] Oxygen neighbors presented in the first coordination shell

Table 4. The Pt distribution determined in the per cm^2 of electrode area

Acronym Name	N_S Total Pt surface atoms per $cm^2/10^{16}$	N_T Total Pt atoms per $cm^2/10^{16}$	Distribution of Pt N_S/N_T (%)
5Ptancr4	13.11	266.2	4.93
5Ptanxcr4[b]	15.11	161.6	9.35
5Ptandr4	8.79	253.8	3.46
15Ptancr4	7.64	52.1	14.66
15Ptanxcr4[b]	7.77	26.4	29.43

[b] Oxygen neighbors presented in the first coordination shell